Research Square

Preprints are preliminary reports that have not undergone peer review.
They should not be considered conclusive, used to inform clinical practice,
or referenced by the media as validated information.

Characterization of the lysine forming saccharopine dehydrogenase LYS1 from filamentous fungi for plant food fermentation

Tomás Vellozo-Echevarría
Technical University of Denmark
Marlene Vuillemin
Technical University of Denmark
Kristian Barrett
Technical University of Denmark
Anne S. Meyer
asme@dtu.dk

Technical University of Denmark

Research Article

Keywords: Lysine, fungi, fermentation, biosynthesis

Posted Date: August 14th, 2026

DOI: https://doi.org/10.21203/rs.3.rs-10420895/v1

License: This work is licensed under a Creative Commons Attribution 4.0 International License.
Read Full License

Additional Declarations: No competing interests reported.

Characterization of the lysine forming saccharopine dehydrogenase LYS1 from filamentous fungi for plant food fermentation

Tomás Vellozo-Echevarría[1], Marlene Vuillemin[1], Kristian Barrett[1], Anne S. Meyer[1*]

[1] Protein and Enzyme Technology Section, Department of Biotechnology and Biomedicine, DTU Bioengineering, Technical University of Denmark, Building 221, DK-2800 Kgs. Lyngby, Denmark

*Corresponding author: asme@dtu.dk

Abstract

Lysine biosynthesis in fungi proceeds through the α-aminoadipate pathway with LYS1 (EC 1.5.1.7) catalyzing the final reversible L-lysine producing step. Although LYS1 from *Saccharomyces cerevisiae* has been characterized, limited information is available on this highly conserved enzyme in filamentous fungi relevant for solid-state food fermentation. Here, we compare LYS1 homologs from *Aspergillus nidulans*, *Penicillium roqueforti*, and *Rhizopus microsporus* with the *S. cerevisiae* enzyme as reference using phylogenetic, biophysical, kinetic, and molecular dynamics analyses. Sequence and structural comparisons showed sequence divergence across fungal lineages while overall fold and key catalytic residues were conserved. All enzymes displayed strong directional pH dependence, with the forward L-lysine producing reaction favored at alkaline pH and the reverse reaction promoted at neutral pH. Analyses of temperature profile revealed homolog-specific differences, with the homolog from *S. cerevisiae* presenting the highest temperature optimum and melting temperature. The turnover (k_{cat}) of the reverse reaction was consistently higher than the forward reaction for all homologs, consistent with thermodynamic constraints on lysine formation. Kinetic characterization revealed that the *S. cerevisiae* enzyme had the highest k_{cat}, followed by *A. nidulans* and *P. roqueforti*, whereas the *R. microsporus* enzyme had lower activity and highest activation energy. Molecular dynamics simulations corroborated that the more active homologs more frequently sampled near-reactive NAD^+ C4-saccharopine C8 geometries, while *R. microsporus* showed lower sampling frequency of these conformations and weaker protein-ligand contact organization. These findings provide a mechanistic and kinetic basis for understanding lysine biosynthesis in filamentous fungi.

Keywords

Lysine; fungi; fermentation; biosynthesis.

Key points

- Phylogenetic, biophysical, kinetic, molecular dynamics of LYS1 from fungi
- Catalytic residues and LYS1 folds are conserved (LDDT >0.9) but sequences differ
- Reaction direction (saccharopine ↔ L-lysine) is strongly dependent on pH

Introduction

Lysine (L-lysine) is an essential amino acid in human nutrition. As plant-based diets keep gaining attention for their reduced environmental impact (Feigin et al., 2025), solid-state fungal fermentation of plant foods is now emerging as a strategy to improve the nutritional and sensory quality of plant-based products through bioconversion (Canoy et al., 2024).

Fungi synthesize lysine naturally through the highly conserved α-aminoadipate (AAA) pathway, which is distinct from the diaminopimelate pathway of bacteria and plants (Bhattacharjee, 1985). This metabolic route uses eight enzymatic steps to catalyze the conversion of α-ketoglutarate (α-KG) to lysine. The final step of the pathway is catalyzed by LYS1 (EC 1.5.1.7), a non-metal, nicotinamide adenine dinucleotide (NAD^+/NADH) dependent oxidoreductase that specifically catalyzes the reversible oxidative deamination of saccharopine to yield lysine and α-KG (Figure 1) (Xu et al., 2006a; Zabriskie & Jackson, 2000). The directionality of the reversible reaction is known to be influenced by the environmental pH. Previous studies have shown that the forward (lysine-forming) reaction is favored under alkaline conditions whereas the reverse (saccharopine-forming) reaction exhibits an optimum at neutral pH (Saunders & Broquist, 1966). Nevertheless, kinetic characterization of the forward reaction has been performed under neutral, suboptimal pH conditions (Xu et al., 2006a). Most of the research on the AAA pathway, including studies on LYS1, has been conducted in model organisms such as *Saccharomyces cerevisiae* and other yeasts. However, filamentous fungi such as *Rhizopus*, *Aspergillus* and *Penicillium* species, which are widely used in traditional solid-state food fermentation processes, including tempeh, miso and cheese production, exhibit lifestyles and metabolic characteristics that differ significantly from those of yeasts (Tamang et al., 2016). Indeed, despite early seminal work on lysine biosynthesis in fungi (Xu et al., 2006a; Zabriskie & Jackson, 2000), the biochemical characterization of LYS1 from different fungi relevant for food fermentation is incomplete.

To fill this knowledge gap, we performed a comparative biochemical characterization of LYS1 homologs from selected fungal species against the *S. cerevisiae* benchmark LYS1 enzyme, focusing on the directional pH dependency, temperature optima and stability, and kinetic analysis of the forward reaction. Structural and molecular dynamics analyses were included to further examine and explain the differences in catalytic behavior.

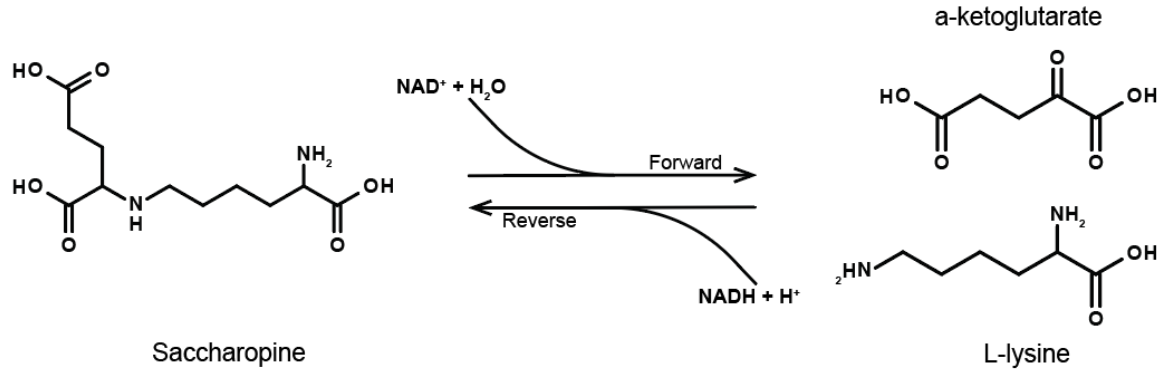


Figure 1. Schematic representation of the reversible reaction catalyzed by LYS1, the last enzyme of the α-aminoadipate pathway for lysine biosynthesis. LYS1 catalyzes the reversible oxidative deamination of saccharopine to yield L-lysine and α-ketoglutarate (α-KG) in the presence of NAD^+, producing NADH and H^+.

Materials and Methods

Sequence retrieval and phylogenetic analysis

Annotated reference genomes from 14 filamentous fungi of relevance for this study were searched for LYS1 enzymes using the amino acid sequence of LYS1 from *S. cerevisiae* (GenBank: X77362.1) as a BLASTp query (v2.17.0+) (Camacho et al., 2009). For each species, the hit with the highest bit-score was selected as the putative ortholog and validated using InterProScan (version 5.77-108.0) for domain detection (Blum et al., 2025). For genomes without annotated proteomes, protein prediction was performed from genome sequences using AUGUSTUS (version 3.5.0) with the closest available model as the reference (Nachtweide & Stanke, 2019). The resulting predicted protein sequences were then used for downstream phylogenetic analysis. Multiple sequence alignment was performed using MAFFT (version 7.490) (Katoh & Standley, 2013). Phylogenetic reconstruction between the selected LYS1 protein sequences was performed using IQ-TREE (version 3.0.1) (Wong et al., 2026). ModelFinder was used for automatic model selection yielding LG+G4 as the optimal substitution model. A maximum-likelihood tree was constructed using SH-aLRT and ultrafast bootstrap with 1000 replicates. Resulting trees and metadata are visualized using iTOL (Letunic & Bork, 2024). Accession numbers and metadata for all sequences used in this study are provided in Supplementary Table S1.

Gene synthesis and plasmid construction

For recombinant enzyme production, each of the LYS1 genes were codon optimized for either *Escherichia coli* or *Pichia pastoris* expression and synthesized by Genscript (Piscataway, NJ,

USA). The sequences for *P. pastoris* expression were cloned into the vector pPICZ(α)A (Invitrogen, Carlsbad, CA, USA) (employing *Eco*RI and *Sal*I restriction sites) to be in frame with the N-terminal α-factor secretion signal from *S. cerevisiae* and a C-terminal His_6-tag. The *S. cerevisiae* sequence was cloned in the bacterial recombinant expression vector pET28a+ (*Nco*I and *Xho*I restriction sites) for *E. coli* expression, also in frame with a C-terminal His_6-tag, as previously described (Xu et al., 2006b). The codon optimized nucleotide sequences and protein IDs have the following Genbank accession numbers: PZ500552 (*S. cerevisiae*), PZ500549 (*R. microsporus*), PZ500550 (*A. nidulans*), PZ500551 (*P. roqueforti*).

Protein expression and purification

Plasmids were transformed into *E. coli* DH5α cells for amplification. Constructs designed for *P. pastoris* expression were then selected on low salt LB agar plates with 100 $\mu g \cdot mL^{-1}$ zeocin (Invitrogen, Carlsbad, CA, USA). Purified plasmids were linearized using the restriction enzyme FastDigest *Mss*I (Thermo Fisher, Waltham, MA, USA) prior to *P. pastoris* transformation by electroporation. Expression was done in *P. pastoris* X-33 using the EasySelect™ *P. pastoris* expression guide (Invitrogen, Carlsbad, CA, USA). Transformants were cultivated at 28 °C in 50 mL buffered glycerol-complex medium (BMGY) containing 100 $\mu g \cdot mL^{-1}$ zeocin. The cells were harvested by centrifugation, inoculated in 500 mL buffered methanol medium (BMMY) with 100 $\mu g \cdot mL^{-1}$ at an $OD_{600\ nm}$ of 1 and cultivated with shaking at 20 °C for 5 days, with addition of methanol (to 1 %) every 24 h. The cells were separated from the supernatant by centrifugation, with the latter containing the enzyme fraction.

For the *E. coli* expression of the *S. cerevisiae* enzyme, the plasmid was transformed into the *E. coli* strain BL21-(DE3) and a colony was picked for preculture in LB medium containing 30 $\mu g \cdot mL^{-1}$ kanamycin. The main culture was inoculated in 500 mL LB, 30 $\mu g \cdot mL^{-1}$ kanamycin, to an $OD_{600\ nm}$ of 0.05 after inoculation. The culture was cultivated at 37 °C with shaking until the $OD_{600\ nm}$ reached approximately 0.8, at which point the culture was induced with the addition of 1 mM IPTG, and the temperature reduced to 23 °C for overnight expression. After 24 hours, the cells were harvested by centrifugation at 4000 g for 15 minutes and the cell pellet was suspended in Ni-Trap binding buffer (Tris HCl 100 mM pH 7; 500 mM NaCl; 50 mM imidazole, pH 7). The cells were then lysed by sonication and the cell fragments spun down at 10,000 g.

Once produced, the enzymes were purified harnessing the His-tag affinity to nickel using 5 mL HisTrap™ FF crude columns (GE Healthcare, UK) with binding buffer and eluted using a linear gradient of 20-250 mM imidazole (Tris HCl 100mM pH 7; 500 mM NaCl; 250 mM imidazole, pH 7). After purification, buffer exchange into storage buffer (Tris HCl 100mM pH 7; 100 mM NaCl, pH 7) was done using PD-10 desalting columns (Cytiva, Merck, Darmstadt, Germany).

The protein solutions were concentrated using Vivaspin® filters (10 kDa cut off) (Sigma-Aldrich, St. Louis, MO, USA), aliquoted into ~100 µL portions and stored at -80 °C.

Enzymatic assay

Unless otherwise specified, the standard forward enzymatic assay was performed using 100 mM Tris HCl (pH 9), 100 mM NaCl, 10 mM NAD+, 5 mM saccharopine, and initiated by the addition of 10 µL of an appropriately diluted enzyme solution. The assay reaction mixture was preheated to the desired temperature (30 °C at the standard condition) prior to addition of the enzyme. Standard determination of enzyme activity in the reverse direction was performed by preincubating 10 µL of an appropriately diluted enzyme solution in 100 mM Tris HCl (pH 7), 100 mM NaCl, 0.2 mM NADH, and 5 mM α-KG. The reaction was initiated by addition of L-lysine to a concentration of 12.5 mM. The final reaction volume was in all cases 50 µL and reactions were carried out in half-area flat bottom 96-well plates. Standard reactions were carried out at 30 °C with orbital shaking (800 cpm) between reads using an Epoch 2 microplate spectrophotometer (BioTek Instruments). Reaction progress was monitored by continuously measuring the appearance/disappearance of NADH as a product of the LYS1 forward/reverse reaction at 340 nm. The initial linear absorbance change obtained was used to calculate the initial rates.

The pH optimality of the forward and reverse LYS1 catalyzed reaction was assessed by measuring the reaction rates at substrate saturating conditions while varying the pH of the reaction buffer (100 mM Tris HCl) from pH 7 to 9 in 0.5 pH steps.

The kinetic parameters of the forward reaction were determined by measuring the initial rates in a matrix of substrate concentrations, varying NAD^+ (0.05, 0.2, 0.5, 1, 5, and 10 mM) at multiple concentrations of saccharopine (0.05, 0.1, 0.5, 1, and 5 mM), and vice versa. Apparent kinetic parameters were obtained by non-linear fitting of the initial rates to the Michaelis-Menten equation at the highest concentration of the co-substrate. Turnover numbers (k_{cat}) were calculated based on the enzyme concentration used.

The reaction activation energy, E_a, and temperature optima were estimated by measuring the rates of the forward reaction (standard assay) at different temperatures between 25 and 50 °C with a step size of 5 °C. The E_a was then determined by linearization of the Arrhenius equation.

The thermal unfolding, T_m, of the enzymes was determined by nano differential scanning fluorimetry (nanoDSF) measuring the progress of fluorescence emission at 330 and 350 nm using a Prometheus™ Panta (NanoTemper Technologies, Munich, Germany). The enzymes were brought to 1.5 µM in 100 mM Tris HCl, 100 mM NaCl, pH 9, mounted in capillary tubes and heated from 20 to 90 °C with a constant heating rate of 1.5 °C per minute.

Structural modeling

Modeling of three-dimensional structure for structure comparison was done using a standalone version of AlphaFold3 (Abramson et al., 2024). For each protein five diffusion samples were generated using three recycling iterations, and the top-ranking model was selected for further structure analyses. All-against-all protein structure comparisons were performed using Foldseek (v10.941) (van Kempen et al., 2024) and the local Distance Difference Test (LDDT) scores (ranging 0-1) were used as a measure of structural similarity.

Molecular dynamics

Molecular dynamics (MD) simulations were performed on four configurations per enzyme (apo, NAD^+ bound, saccharopine bound, and ternary complex) each simulated in triplicate. Three-dimensional structures of NAD^+ and saccharopine bound LYS1 were predicted using AlphaFold3 as previously described and the top-ranking model was selected and prepared for simulation. NAD^+ and saccharopine were included in the respective systems based on AlphaFold3 predicted coordinates and parameterized using CHARMM General Force Field (CGenFF 4.6, https://cgenff.com/, accessed 10th of April 2025). Local pK_a information was derived from PropKa3 to assign protonation states at pH 9 (mimicking the forward reaction conditions). Systems were parameterized in GROMACS (version 2023.3) using the Charmm36 all-atom force field (July 2022) with the CHARMM-modified TIP3P water model (Abraham et al., 2015; Huang & MacKerell, 2013; MacKerell et al., 1998). Solvation was performed in dodecahedral boxes and neutralized with 0.15 M NaCl. Initial minimization of the system was performed using a steepest descent approach until the maximum force was below 1000 $kJ \cdot mol^{-1} \cdot nm^{-1}$. After, NVT equilibration (300 K) was performed for 100 ps, followed by an NPT equilibration (300 K, 1.0 bar) for 100 ps. The systems were then subject to MD simulations for 100 ns under NPT conditions using a leap-frog integrator, V-rescale thermostat, and Parrinello-Rahman barostat.

Statistical analysis

Measurements of enzymatic activity and reaction optimality were performed in triplicate and reported as mean ± SD. Non-linear regression to the Michaelis-Menten equation was performed on the initial rate data using varying concentrations of the substrate and cofactor, kinetic parameters are reported as mean ± SE. Statistical comparisons between homologs were performed using two-tailed Student's t-tests ($p < 0.05$).

For molecular dynamics analysis each system was simulated in triplicate. RMSD, RMSF, catalytic distance frame frequencies, and contact occupancies, were calculated independently for each replicate and summarized as mean ± SD. Residue contact occupancy vectors were

z-scored for generation of the protein-ligand contact PCA, where contact features were retained when occupancy was >10% in at least one replicate, non-zero variance, and a F-ratio (between-species variance to within-species variance) ≥1.5.

Results

Sequence comparison of LYS1 enzymes

Phylogenetic analysis of the selected LYS1 sequences revealed clear clades representing the different genera and an evident separation between the *S. cerevisiae* enzyme and the filamentous fungi homologs (Figure 2). *Aspergillus* and *Penicillium* LYS1 grouped together and separate from those of *Rhizopus*. This was analogously reflected in pairwise sequence similarities (Supplementary Table S2), with high similarity observed within each genus (up to 99.5%), and considerable conservation across *Aspergillus* and *Penicillium* (~80 - 85%). Lower degrees of similarity were observed between the *Aspergillus* and *Penicillium* versus the *Rhizopus* homologs (~54.4 - 58.7%), and *S. cerevisiae* (~53.8 - 55.4%), respectively (Supplementary Table S2). The sequence alignment showed varying conservation patterns distributed through the sequence with small genera and species-specific insertions, strongly conserved residues, and regions of significant sequence diversity (Supplementary Figure S1).

Structural comparison based on models predicted with AlphaFold3 showed high similarity across all enzymes (Figure 2). Pairwise LDDT values were thus all above 0.9 pointing to a high fold conservation of the analyzed LYS1 enzymes. Structural distances also reveal clades between and within the genera, where the *Aspergillus* and *Penicillium* show higher structural similarity to each other than to the *Rhizopus* homologs. Almost identical folds were seen within the *Rhizopus* and the *Penicillium* genera.

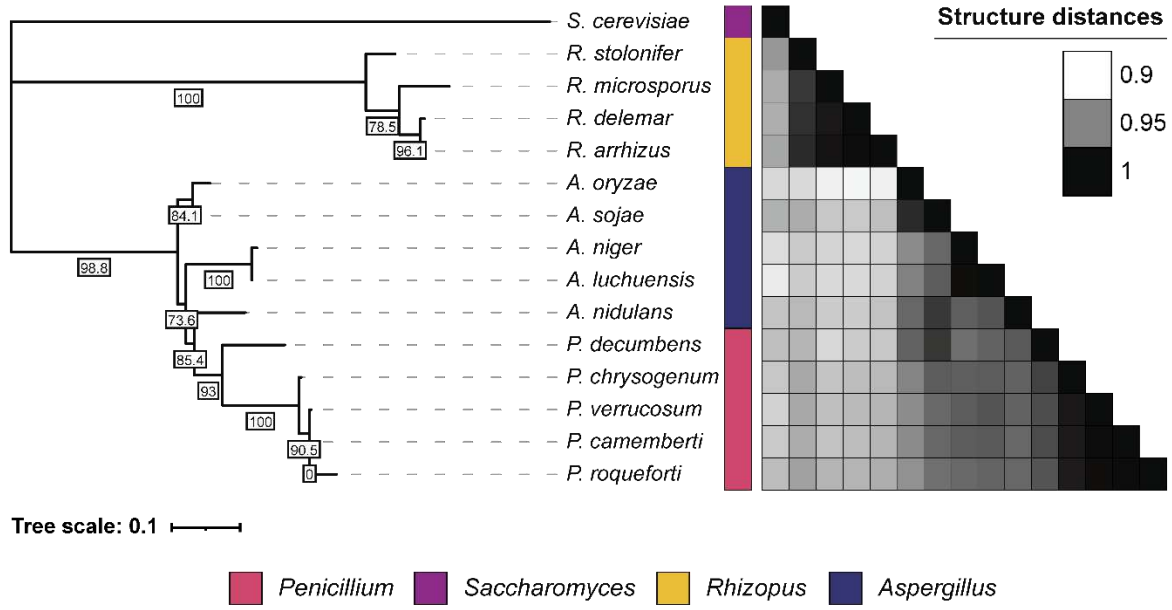


Figure 2. Phylogenetic and structural comparison of selected fungal LYS1 enzymes. (Left) Maximum-likelihood phylogeny of LYS1 protein sequences from 14 fungal species. Branch support values (shown in white boxes) correspond to ultrafast bootstrap (1000 replicates), the tree scale indicates substitutions per site. Genera are grouped by color annotations. (Right) Pairwise structural similarity matrix of predicted LYS1 models shown as local Distance Difference Test (LDDT) scores (0–1), higher values indicate higher structural similarity.

pH profile of the forward and reverse reactions

The catalytic activity measured for the expressed LYS1 enzymes showed a high dependence on the pH of the reaction. The forward reaction consistently showed increased k_{cat} with increased pH, a maximum being observed at pH value of 9 (Figure 3, A). In contrast, the reverse reaction presented an optimal at neutral pH with activity declining as alkalinity increased (Figure 3, B). The *R. microsporus* enzyme showed considerably lower activity as compared to the Ascomycete enzymes, with an average 30-fold and 63-fold lower k_{cat} in the forward and reverse reaction, respectively. Significantly higher k_{cat} values were measured in the reverse reaction as compared to the forward reaction, regardless of the pH conditions tested. Thermodynamic estimates of the reaction free energy predict the forward reaction to be energetically unfavorable under both neutral and alkaline conditions ($\Delta_r G'^m$ ≈ +19.5 and +9.1 kJ·mol^{-1} at pH 7 and 9, respectively), whereas the reverse reaction is correspondingly favorable ($\Delta_r G'^m$ ≈ -19.5 and -9.1 kJ·mol^{-1} at pH 7 and 9, respectively) (Beber et al., 2022).

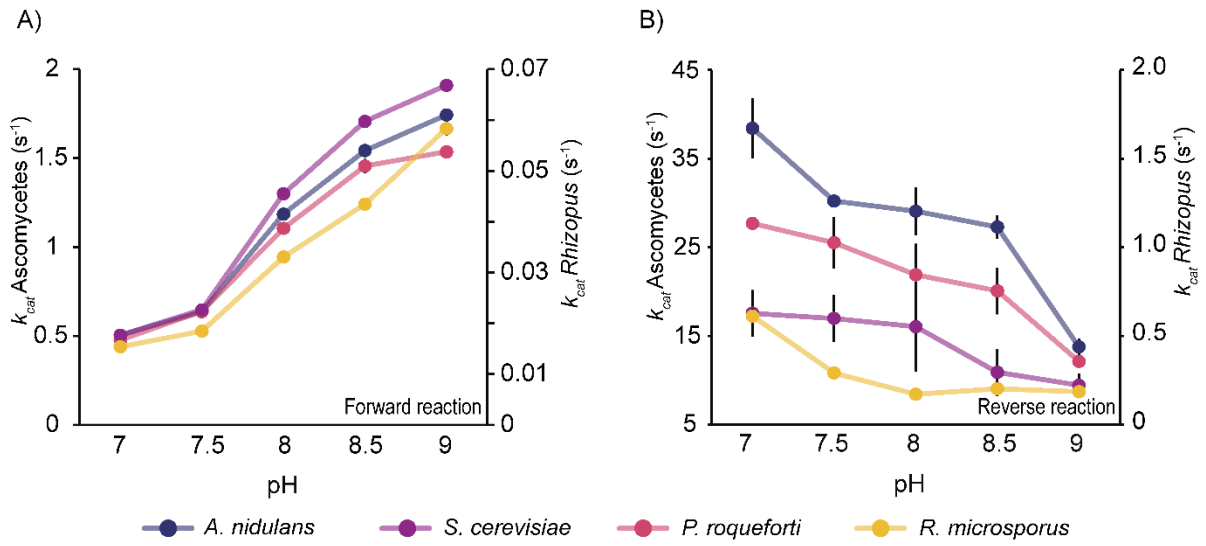
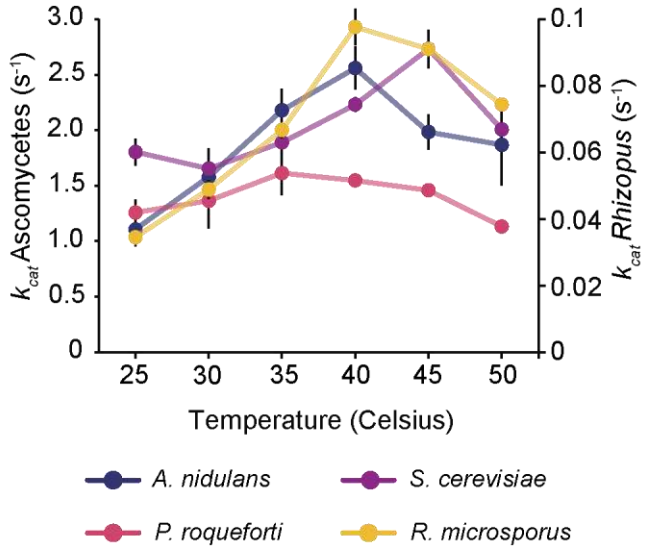


Figure 3. pH profile of LYS1 k_{cat} in the forward and reverse reactions. k_{cat} of LYS1 homologs measured from pH 7 to 9 in a 0.5 step under saturating concentrations of substrates and cofactors. Left y-axis depicts the k_{cat} values corresponding to the Ascomycete LYS1 homologs, right y-axis shows the Rhizopus LYS1 homolog k_{cat}. A) Forward reaction, k_{cat} increases toward alkaline pH. B) Reverse reaction, maximal k_{cat} near neutral pH and decreasing activity at higher pH. Values are given as mean ± SD of triplicate measurements.

Temperature reaction optima and thermal denaturation profile

Analysis of the temperature optimality of the forward reaction and the melting temperatures revealed further differences between the LYS1 homologs (Figure 4). The enzyme from *S. cerevisiae* presented the highest optimal temperature (at 45 °C), consistent with its higher melting temperature and temperature denaturation onset (T_m ~ 60 °C). The enzyme from the different fungi displayed lower optimal temperatures, i.e. 40 °C for the *A. nidulans* and *R. microsporus* homologs, and 35 °C for the *P. roqueforti* LYS1.



253

	T_m °C	T_{ON} °C
A. nidulans	47.3 ± 0.04[a]	38.7 ± 0.29[a]
P. roqueforti	39.6 ± 0.05[b]	31.6 ± 1.02[b]
S. cerevisiae	59.9 ± 0.10[c]	45.9 ± 1.31[c]
R. microsporus	46.7 ± 0.85[a]	32.8 ± 1.73[b]

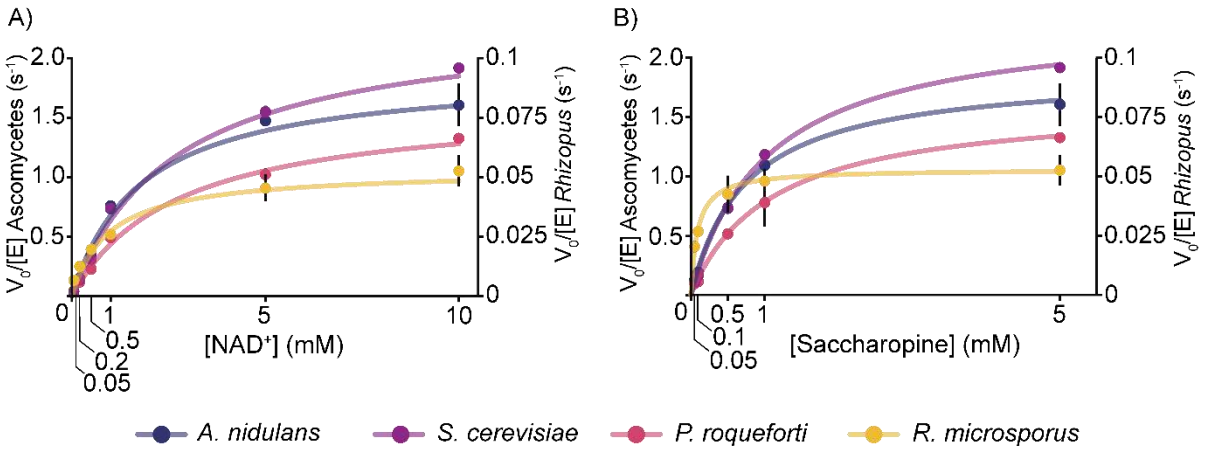
254 Figure 4. Temperature dependence of LYS1 catalysis and robustness of LYS1 of different
255 fungal origin. (Top) Temperature profile of the k_{cat} of LYS1 homologs measured from 25 to 50
256 °C under saturating concentrations of substrates and cofactors. Left y-axis depicts the k_{cat}
257 values corresponding to the Ascomycete LYS1 homologs, right y-axis shows the k_{cat} of the
258 *Rhizopus* LYS1 homolog. (Bottom) Thermal stability parameters determined by nanoDSF. The
259 unfolding ("melting") temperature (T_m) and onset temperature of unfolding (T_{ON}) for the LYS1
260 homologs. Values are reported as mean ± SD of triplicate measurements. Different superscript
261 letters within each column indicate statistically significant differences between LYS1 homologs
262 (two-tailed Student's t-test, $p < 0.05$).

263 Kinetic characterization of the forward reaction

264 Kinetic characterization of the forward reaction revealed important differences in the catalytic
265 efficiencies of the tested LYS1 homologs (Figure 5, A and B). The enzyme from *S. cerevisiae*
266 presented the highest k_{cat} (k_{cat} 2.3 s^{-1}), followed by *A. nidulans* and *P. roqueforti*. As previously
267 described, the *R. microsporus* homolog showed significantly reduced activity (k_{cat} 0.05 s^{-1}).
268 The *R. microsporus* homolog displayed lower apparent K_M for NAD^+ and saccharopine (K_{NAD^+}
269 0.94 mM and K_{sacc} 0.09 mM) as compared to the Ascomycete enzymes which showed higher
270 K_M values for both substrates and higher catalytic efficiencies, where the *A. nidulans* and *S.*
271 *cerevisiae* enzymes exhibited the highest efficiency, followed by that of *P. roqueforti* (Figure
272 5).

The calculated activation energy values support these observations. The slowest enzyme, *R. microsporus* LYS1, showed the highest E_a, indicating a higher energy barrier. Conversely, the fastest enzyme, *S. cerevisiae* LYS1, showed the lowest E_a values, consistent with its better catalytic performance (Supplementary Figure S2).

The substrate matrix tested reveals cosubstrate dependence of LYS1 with the apparent k_{cat} being increased with addition of both substrates and with maximal turnover requiring sufficient availability of NAD^+ and saccharopine (Supplementary Figure S3). Hanes-Woolf linearization of the Michaelis-Menten data on the substrate matrix showed intersecting lines with variation of NAD^+ and saccharopine (Supplementary Figure S4), consistent with a sequential mechanism proceeding after the establishment of a ternary complex.



LYS1	k_{cat} s^{-1}	K_{NAD^+} mM	k_{cat}/K_{NAD^+}	K_{sacc} mM	k_{cat}/K_{sacc}	E_a kJ·mol^{-1}
A. nidulans	1.89 ± 0.03^a	1.78 ± 0.15^a	1.06 ± 0.07^a	0.74 ± 0.04^a	2.54 ± 0.11^a	27.6 ± 1.8^a
P. roqueforti	1.63 ± 0.03^b	2.72 ± 0.26^b	0.60 ± 0.05^b	1.07 ± 0.08^b	1.52 ± 0.08^b	20.3 ± 1.4^b
S. cerevisiae	2.34 ± 0.02^c	2.67 ± 0.18^b	0.88 ± 0.05^a	1.03 ± 0.03^b	2.27 ± 0.05^a	13.1 ± 0.5^c
R. microsporus	0.05 ± 0.00^d	0.94 ± 0.16^c	0.06 ± 0.01^c	0.09 ± 0.01^c	0.59 ± 0.06^c	53.3 ± 1.3^d

Figure 5. Single substrate Michaelis-Menten forward kinetic characterization of LYS1 homologs. (A) Dependence of the initial rate divided by the total enzyme concentration (V_0/[E]) on NAD^+ concentration (0.05, 0.2, 0.5, 1, 5, and 10 mM) measured at saturating saccharopine (5 mM). (B) V_0/[E] dependence on saccharopine (0.05, 0.1, 0.5, 1, 5 mM) concentration measured at saturating NAD^+ (10 mM). Left y-axis depicts the V_0/[E] values corresponding to the Ascomycete LYS1 homologs, right y-axis shows the *Rhizopus* LYS1 homolog V_0/[E]. Non-

linear fitting to the Michaelis-Menten equation was done to obtain apparent kinetic parameters. Values are reported as mean ± SE from triplicate measurements. The table summarizes the kinetic parameters derived from non-linear fits, including k_{cat}, apparent Michaelis constants for NAD^+ (K_{NAD^+}) and saccharopine (K_{sacc}), catalytic efficiencies (k_{cat}/K_{NAD^+} and k_{cat}/K_{sacc}), and activation energies (E_a) calculated from linearization of the Arrhenius equation with data from activity measured at different temperatures. Different superscript letters within each column indicate statistically significant differences between LYS1 homologs (two-tailed Student's t-test, $p < 0.05$).

Molecular dynamics of LYS1-substrate complexes

MD simulations were performed for the four experimentally characterized LYS1 homologs to investigate the molecular mechanisms underlying the observed kinetic differences. Simulations were performed for the apo, NAD^+-bound, saccharopine-bound, and ternary systems. The distance between the C4 atom of NADH and the C8 atom of saccharopine was previously reported to be 3.6 Å, a distance compatible with hydride transfer (Kumar et al., 2012). Therefore, this distance was measured in this study as a proxy for the ability of the homologs to sample appropriate hydride transfer distance in the ternary complex. A depiction of the mentioned distance can be seen in Figure 6 B. To account for thermal fluctuations during MD, the frequency of frames was calculated for the distance of the NAD^+ C4 to saccharopine C8 using 4.5, 4.0 and 3.6 Å thresholds representing a relaxed proximal conformation, a near-catalytic distance, and the reported hydride transfer catalytic distance, respectively.

The frequency of frames below said thresholds differed among homologs (Figure 6 A). The frequency below 4.5 Å was highest for the LYS1 of *S. cerevisiae* (9.5%) and *A. nidulans* (8.7%), followed by *P. roqueforti* (5.1%) and *R. microsporus* (3.4%). A similar trend was observed at the 4.0 Å threshold with *A. nidulans* showing the highest frequency (3.4%), followed by *S. cerevisiae* (1.8%), *P. roqueforti* (1.3%), and *R. microsporus* (0.6%). Frames with distances below the experimental distance of 3.6 Å were scarce in all systems but showed a similar pattern with *A. nidulans* showing the highest frequency (0.34%) and *R. microsporus* the lowest (0.08%).

Measurements of the RMSD of the apo backbone indicated global stability throughout the 100 ns of simulation while showing differences in the general backbone flexibility between the homologs (Figure 6 C). In the apo state, *S. cerevisiae* presented the most rigid structure, with an RMSD of 3.1 ± 0.2 Å, while the *P. roqueforti* and *A. nidulans* showed more flexibility, 3.5 ± 0.2 Å and 3.6 ± 0.8 Å, respectively. The *R. microsporus* enzyme showed the highest RMSD and variability with 3.8 ± 1.1 Å.

These differences were similarly supported by the active site RMSF (Figure 6 D), where *S. cerevisiae* showed low active site flexibility in the apo state and little change in the flexibility upon ternary complex formation (ΔRMSF = -0.1 ± 0.2 Å). Conversely, the filamentous fungi showed sharper decreases in the active site RMSF in the ternary state (e.g. *A. nidulans* ΔRMSF = -0.5 ± 0.4 Å, Supplementary Table S3), indicative of stronger rigidification of the active site upon substrate binding.

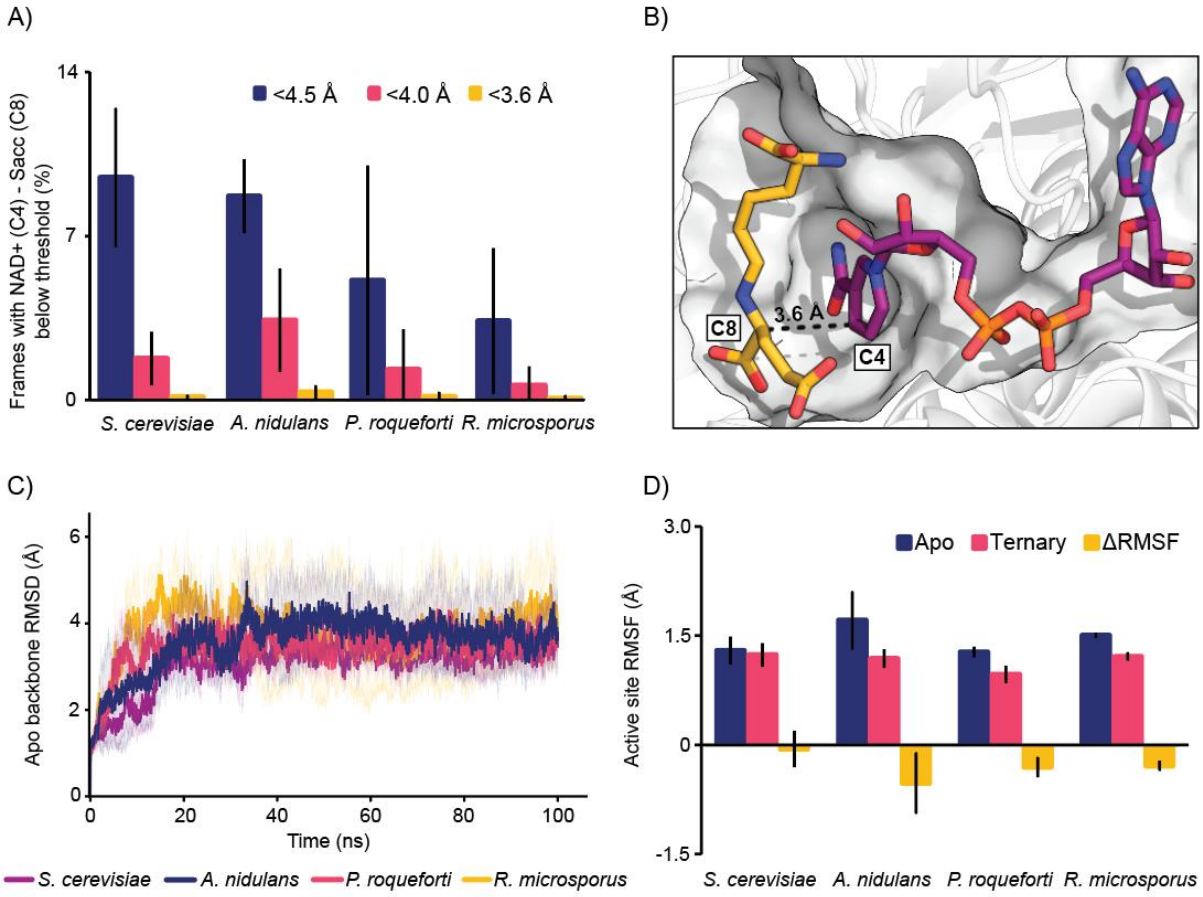


Figure 6. Molecular dynamics analysis of LYS1 homologs in ternary and apo states. (A) Frequency of ternary complexes simulation frames with distances between NAD^+ C4 and saccharopine C8 below 4.5, 4.0, and 3.6 Å thresholds, representative of proximal relaxed, near-catalytic, and reported hydride transfer catalytic distance, respectively. Values are reported as mean ± SD from three independent simulations per complex. (B) Representative frame of the LYS1 homolog from *A. nidulans* showing the ternary complex active site in presence of NAD^+ and saccharopine with the measured NAD^+ C4 to saccharopine C8 distance highlighted. (C) RMSD profiles of the apo backbone for the LYS1 homologs throughout 100 ns of simulation. Mean shown as lines with transparent shading for the SD across triplicate simulations. (D) RMSF of the Cα of the active site in the apo and ternary complexes through simulations, ΔRMSF was calculated as ternary RMSF minus apo RMSF. Values are reported as mean ± SD from three independent simulations per complex.

Protein-ligand contacts were further analyzed to understand differential substrate contact organization strategies between homologs. Principal component analysis of the fingerprints for residue level contact occupancy of the homologs separated the ternary complexes (Figure 7 A). PC1 explained 34.4% of variance and mainly separated *P. roqueforti* from the rest of the homologs while being enriched in saccharopine contact features, whereas PC2 explained 25.2% of variance and was enriched in NAD^+ contact features (Figure 7 B, Supplementary Table S4).

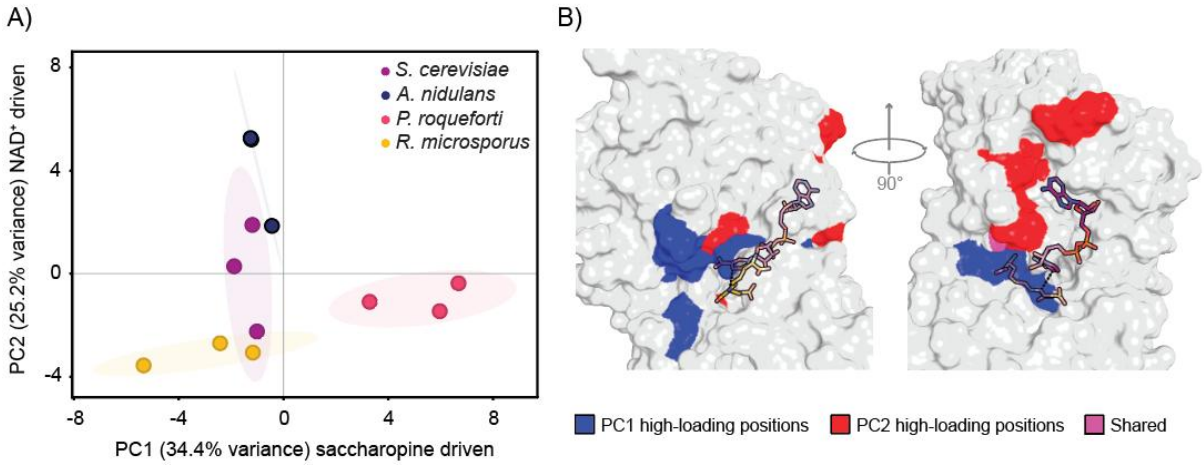


Figure 7. Contact organization between protein and ligand in LYS1 ternary complexes. (A) Principal component analysis derived from z-scored contact occupancy vectors across four LYS1 homologs in triplicate simulations. Each point represents one replicate. Features were retained by occupancy (≥ 10% in one replicate), zero-variance, and F-ratio filters (between-species variance/within-species replicate variance ≥ 1.5). (B) Structural mapping of high loading positions onto a representative frame of the LYS1 homolog from *A. nidulans* showing the ternary complex. Residues contributing above the average loading value for PC1 are shown in blue, residues contributing to PC2 in red, and residues contributing to both in magenta.

This separation is further supported by the quantification of the number of residues with persistent contact in the ternary complex (Supplementary Table S5). *R. microsporus* showed the lowest number of residues with more than 50% NAD^+ occupancy (19), compared with *A. nidulans* (24), *P. roqueforti* (23), and *S. cerevisiae* (21). Conversely, *P. roqueforti* showed the most persistent contacts with saccharopine in the ternary state (18), compared to *A. nidulans* (11), *R. microsporus* (10), and *S. cerevisiae* (9). The contact occupancies of saccharopine and NAD^+ were mapped onto an alignment of the sequences of interest, revealing general concentration of the contacts around conserved regions, as expected from an active site function preservation perspective (Supplementary Figure S5 and Figure S6).

Discussion

The vast majority of the research regarding LYS1, crucial last step of the AA pathway for lysine biosynthesis, and its mode of action and has been conducted using the homolog from *S. cerevisiae*. To expand on the sequence space, sequence comparison and phylogenetic analysis of selected LYS1 enzymes from relevant filamentous fungi revealed clear clades to the genus level. Some patterns expected from phylogenetic relationships were clearly observed, i.e. clade proximity and sequence similarity between *Aspergillus* and *Penicillium* homologs and separation with the *Rhizopus* clade (Figure 2). Pairwise sequence similarity values confirmed this pattern and evidenced a markedly low sequence similarity between the filamentous fungi homologs and the *S. cerevisiae* counterpart. The Mucoromycete and the filamentous Ascomycete homologs showed comparable low degrees of similarity with the yeast enzyme (~50 and 55%, respectively, Supplementary Table S2), striking as a clear sequence diversification of the yeast homolog within the Ascomycota phylum (Li et al. 2021). These observations are further confirmed by the comparison of the predicted structures of the enzymes, which, regardless of the high structural similarity, produced clades similar to the sequence-based analysis. Despite the observed sequence differences, previously described catalytic residues Lys77, His96, and Glu122 were conserved across all the sequences, as well as Lys99 and Asp281 which have been reported to contribute to conformational changes (alignment positions 89, 108, 122, 111, and 296, respectively, Supplementary Figure S1). Similarly, Arg18 and Arg131 which have been shown to interact with saccharopine, and Cys205 and Cys249 which form a disulfide bond in the *S. cerevisiae* homolog were found to be conserved in the aligned sequences (Burk et al. 2007; Kumar et al. 2012). Although this conservation is consistent with general preservation of catalytic features, the significant sequence divergence as compared to the *S. cerevisiae* homolog highlights the importance of detailed characterization of LYS1 from filamentous fungi in order to properly understand lysine biosynthesis in fermentation systems.

The reaction catalyzed by LYS1 is known to be reversible and highly pH dependent. The experimentally tested LYS1 homologs show strong pH dependence (Figure 3), in accordance with previous characterization studies of LYS1 from *S. cerevisiae*, where the forward reaction showed an optimum at the maximum pH tested of 10 and the reverse optimality was around pH 7 (Saunders & Broquist, 1966). Later studies incorporated this pH dependency into mechanistic studies of the LYS1 from *S. cerevisiae*, associating substrate binding and catalysis to ionizable groups (Xu et al., 2007). Interestingly, all the enzymes assessed experimentally in this study showed significantly higher k_{cat} values in the reverse reaction as compared to the forward reaction, even when comparing suboptimal pH conditions of the reverse reaction against optimal conditions of the forward reaction. Previous reports of LYS1

from *S. cerevisiae* have also shown several folds higher k_{cat} values for the reverse reaction, with measured values of 1.1 s^{-1} versus 20 s^{-1} in the forward and reverse reaction, respectively (Xu et al., 2006b). This suggests a catalytic preference of the enzymes for the reverse reaction, which may be reflected by thermodynamic constraints of the reaction. Theoretical thermodynamic estimates predict the forward reaction to be energetically unfavorable in opposition to a favorable reverse reaction, and while alkaline pH is predicted to reduce the thermodynamic barrier of the forward reaction, the reaction remains endergonic (Beber et al., 2022). This suggests that the success of the LYS1 forward reaction flux likely depends on intracellular metabolite concentrations and pathway coupling for lysine production.

As mentioned earlier, most of the characterization performed on the forward reaction catalyzed by LYS1 has been carried out at pH 7. Due to the strong pH dependency of the reaction favoring alkaline conditions in the forward sense, these constitute enzyme characterizations at suboptimal conditions. Previous analyses of the forward reaction on the *S. cerevisiae* homolog have reported k_{cat} values of 1.1 s^{-1} at 25 °C and pH 7 (Xu et al., 2006b). The k_{cat} measured here for the *S. cerevisiae* LYS1 was slightly higher (k_{cat} 2.3 s^{-1}), and, while differences in assay temperature should be noted, the higher measured k_{cat} is consistent with the reported pH dependency of the forward reaction (Figure 5). Similarly, previous analyses of the forward reaction performed at pH 7 on the *S. cerevisiae* homolog reported apparent K_M values of 0.9 and 6.7 mM for NAD^+ and saccharopine, respectively, while an earlier study under similar pH conditions reported lower values of 0.1 and 1.67 mM (Fujioka & Nakatani, 1970; Xu et al., 2006b). There, the apparent K_M was lower for NAD^+ than for saccharopine in both cases, suggesting that the enzyme reaches NAD^+ saturation faster than saccharopine saturation under neutral conditions. Under the hereby tested alkaline conditions for the forward reaction, the *S. cerevisiae* homolog showed an apparent K_M of 2.67 mM for NAD^+ and 1.03 mM for saccharopine, switching the substrate saturation pattern (Figure 5). This could be indicative of alkaline pH altering the kinetic balance between cofactor and substrate. Comparatively, significantly lower k_{cat} was measured for the *R. microsporus* enzyme in both directions of the reaction as compared to the Ascomycete enzymes. This, in combination with a lower apparent K_M for NAD^+ and saccharopine, could point to tight substrate binding but a potential catalytic bottleneck in the turnover resulting in a species-dependent limitation in lysine biosynthesis in *Rhizopus*. Although different catalytic efficiencies could be observed, a sequential mechanism was proven to be conserved in all fungal homologs in this study. Studies with the enzyme from *S. cerevisiae* have previously demonstrated an ordered sequential mechanism, with NAD^+ binding before saccharopine, supporting the idea that cofactor availability could be an important factor for forward catalysis (Xu et al., 2006b).

Furthermore, differences in temperature optimality and melting temperatures suggest significant biophysical diversification regardless of the conservation of catalytic function (Figure 4). The observed trend could broadly reflect the ecological and physiological temperature ranges of the source organisms, with the known growth optima of these fungi reported to be around 32 °C with tolerance up to 45 °C for *S. cerevisiae*, 25 °C for *P. roqueforti*, 35 °C for *A. nidulans*, and 40 °C for *R. microsporus* (Coton et al., 2020; Han & Nout, 2000; Panasenko, 1967; Salvadó et al., 2011).

To elucidate the possible mechanisms behind the experimentally observed kinetic differences between homologs, molecular dynamics simulations were performed on the relevant structures in the bound and unbound states. Backbone flexibility, in the form of RMSD of the unbound state, varied between the different homologs, where *S. cerevisiae* presented the most rigid structure and *R. microsporus* the most flexible through the simulation. This rigidity of the yeast enzyme could explain the significantly higher melting temperature of this homolog as compared to the filamentous fungi (Figure 6 C). Moreover, this suggests intrinsic differences in the conformational behavior between homologs, where variations in flexibility could influence substrate binding and effective catalytic conformations.

Further analysis of the active site flexibility, as measured by changes in the RMSF of active site residues, revealed increased rigidity in the ternary complex compared to the apo state. The extent of the rigidification of these residues was variable, with the filamentous fungi homologs presenting stronger rigidification upon substrate binding (Figure 6 D). This effect upon binding is consistent with structural studies of the *S. cerevisiae* homolog showing that active site cleft closure is necessary for ternary complex formation, although the extent of this difference has never been experimentally confirmed between enzyme homologs (Burk et al., 2007; Kumar et al., 2012). The closure produces the assembly of NADH, saccharopine, and catalytic residues K77 and H96 in the ternary complex, where the C4 atom of NADH and the C8 atom of saccharopine are brought to a catalytic distance of 3.6 Å (Figure 6 B) (Kumar et al., 2012). The frequency of frames these two atoms positioned at distances below 4.5, 4.0 and 3.6 Å thresholds were measured, representing increasingly closer states to the expected catalytic distance. The frequency of frames below these thresholds was higher for the more active LYS1 enzymes and lower for the less active one (Figure 6 A). These results indicate that the more active LYS1 homologs, *A. nidulans* and *S. cerevisiae*, sample more frequently near reactive substrate-cofactor geometries than the low activity enzyme, namely the *R. microsporus* homolog.

The residue-level contact frequencies between protein and ligands were used to produce a principal component analysis that revealed distinct occupancy patterns between the homologs

despite the conservation of sequence and fold (Figure 7). Furthermore, the less active enzyme from *R. microsporus* showed the lowest NAD^+ residue occupancy. This reduced contact could be partially explanatory of the reduced capabilities of the *R. microsporus* homolog to effectively position the cofactor and the substrate at an appropriate reaction distance. These differences in protein-ligand interaction highlight the importance of surrounding or distant residues in the stabilization of reactant contacts, while also bringing light into several regions of relevance for substrate contact in LYS1. The contact maps were also in accordance with the crystallographic evidence pointing to Lys77 (in this study alignment position 84), His96 (position 103), and Glu122 (position 129) as relevant residues for catalysis and in contact with saccharopine (Burk et al., 2007; Kumar et al., 2012; Xu et al., 2007). Although binding architecture is similar between homologs, and considering that contact occupancy is not exclusively related to catalytic efficiency, an important substitution Ala289Cys in the *R. microsporus* homolog could potentially hinder the contacts in the vicinity of the hydride transfer region (Supplementary Figure S5 and Figure S6).

Altogether, this analysis suggests that differences in kinetic rates arise from differences in the successful occupancy and organization of productive, protein-ligand interactions. Overall, the MD suggests that kinetic differences could be linked to variation in the ternary complex organization, with particular relevance found in the substrate-contact patterns for effective achievement of the appropriate (short) distance between reactants and enzyme contact.

Conclusions

This study shows that fungal LYS1 homologs are biochemically diverse, despite high structural conservation. Previously reported pH directionality shown for *S. cerevisiae* was confirmed for the recombinantly expressed homologs. The predominant preference observed for the reverse reaction could reflect the thermodynamic constraint of the production of lysine from saccharopine. Interestingly, the forward lysine-forming catalytic reaction is favored in alkaline pH which could pose a pathway context constraint on the actual subcellular localization of LYS1 to an environment where cofactor dynamics and proton concentrations are controlled, e.g. the peroxisomes. The forward reaction showed catalytic diversification among homologs, where the Ascomycete enzymes displayed higher turnover and catalytic efficiency than the *R. microsporus* enzyme. Due to the reversible nature of this terminal step of the pathway and the reported product inhibition mechanisms, LYS1 is hypothesized to directly influence the biosynthetic flux and lysine output. Molecular dynamics analyses data supports a model in which LYS1 catalytic divergence arises from differences in ternary complex organization rather than from loss of the catalytic scaffold. While LYS1 is not the only factor in play in the final lysine concentration in a fermentation product, these results suggest that *R. microsporus* LYS1

could have a catalytic bottleneck in lysine biosynthesis. The data obtained thus provide a mechanistic basis for understanding lysine biosynthesis in fungi relevant for solid-state fermentation and may have implications for selecting non-*Rhizopus* strains for such fermentations.

Data availability

All data supporting the findings of this study are available within the paper and its Supplementary Information.

Author contributions

TV-E, MV, KB, and ASM conceived and designed research. TV-E and MV conducted experiments. TV-E analyzed the data. TV-E, KB, and ASM wrote the manuscript. All authors read and approved the manuscript.

Funding

This work was supported by the project PROFERMENT: Solid-state fermentations for protein transformations and palatability of plant-based foods (grant from the Novo Nordisk Foundation NNF21OC0066330).

Declarations

Conflict of Interest

The authors declare no conflicts of interest.

Ethical approval

No ethical approval was needed for this work.

References

Abraham MJ, Murtola T, Schulz R, Páll S, Smith JC, Hess B, Lindahl E (2015) GROMACS: High performance molecular simulations through multi-level parallelism from laptops to supercomputers. SoftwareX 1-2:19-25. doi: 10.1016/j.softx.2015.06.001

Abramson J, Adler J, Dunger J, Evans R, Green T, Pritzel A, Ronneberger O, Willmore L, Ballard AJ, Bambrick J, Bodenstein SW, Evans DA, Hung CC, O'Neill M, Reiman D, Tunyasuvunakool K, Wu Z, Žemgulytė A, Arvaniti E, Beattie C, Bertolli O, Bridgland A, Cherepanov A, Congreve M, Cowen-Rivers AI, Cowie A, Figurnov M, Fuchs FB, Gladman H, Jain R, Khan YA, Low CMR, Perlin K, Potapenko A, Savy P, Singh S, Stecula A, Thillaisundaram A, Tong C, Yakneen S, Zhong ED, Zielinski M, Žídek A, Bapst V, Kohli P, Jaderberg M, Hassabis D, Jumper JM (2024) Accurate structure prediction of biomolecular interactions with AlphaFold3. Nature 630:493-500. doi: 10.1038/s41586-024-07487-w

Beber ME, Gollub MG, Mozaffari D, Shebek KM, Flamholz AI, Milo R, Noor E (2022) eQuilibrator 3.0: A database solution for thermodynamic constant estimation. Nucleic Acids Res 50:D603-D609. doi: 10.1093/nar/gkab1106

Bhattacharjee JK (1985) α-Aminoadipate pathway for the biosynthesis of lysine in lower eukaryotes. CRC Crit Rev Microbiol 12:131-151. doi: 10.3109/10408418509104427

Blum M, Andreeva A, Florentino LC, Chuguransky SR, Grego T, Hobbs E, Pinto BL, Orr A, Paysan-Lafosse T, Ponamareva I, Salazar GA, Bordin N, Bork P, Bridge A, Colwell L, Gough J, Haft DH, Letunic I, Llinares-López F, Marchler-Bauer A, Meng-Papaxanthos L, Mi H, Natale DA, Orengo CA, Pandurangan AP, Piovesan D, Rivoire C, Sigrist CJA, Thanki N, Thibaud-Nissen F, Thomas PD, Tosatto SCE, Wu CH, Bateman A (2025) InterPro: The protein sequence classification resource in 2025. Nucleic Acids Res 53:D444-D456. doi: 10.1093/nar/gkae1082

Burk DL, Hwang J, Kwok E, Marrone L, Goodfellow V, Dmitrienko GI, Berghuis AM (2007) Structural studies of the final enzyme in the α-aminoadipate pathway-saccharopine dehydrogenase from *Saccharomyces cerevisiae*. J Mol Biol 373:745-754. doi: 10.1016/j.jmb.2007.08.044

Camacho C, Coulouris G, Avagyan V, Ma N, Papadopoulos J, Bealer K, Madden TL (2009) BLAST+: Architecture and applications. BMC Bioinformatics 10:421. doi: 10.1186/1471-2105-10-421

565 Canoy TS, Wiedenbein ES, Bredie WLP, Meyer AS, Wösten HAB, Nielsen DS (2024)
566 Solid-state fermented plant foods as new protein sources. Annu Rev Food Sci Technol
567 15:189-210. doi: 10.1146/annurev-food-060721-013526

568 Coton E, Coton M, Hymery N, Mounier J, Jany JL (2020) *Penicillium roqueforti*: An
569 overview of its genetics, physiology, metabolism and biotechnological applications.
570 Fungal Biol Rev 34:59–73. doi: 10.1016/j.fbr.2020.03.001

571 Feigin SV, Wiebers DO, Blumstein DT, Knight A, Eshel G, Lueddeke G, Kopnina H, Feigin
572 VL, Morand S, Lee K, Brainin M, Shackelford TK, Alexander SM, Marcum J, Merskin D,
573 Skerratt LF, Van Kleef GA, Whitfort A, Freeman CP, Winkler AS (2025) Solving climate
574 change requires changing our food systems. *Oxf Open Clim Change*, *5*(1): kgae024. doi:
575 10.1093/oxfclm/kgae024

576 Fujioka M, Nakatani Y (1970) A kinetic study of saccharopine dehydrogenase reaction.
577 Eur J Biochem 16:180-186. doi: 10.1111/j.1432-1033.1970.tb01070.x

578 Han BZ, Nout RMJ (2000) Effects of temperature, water activity and gas atmosphere on
579 mycelial growth of tempe fungi *Rhizopus microsporus* var. *microsporus* and *R.*
580 *microsporus* var. *oligosporus*. World J Microbiol Biotechnol 16:853-858. doi:
581 10.1023/A:1008974621698

582 Huang J, MacKerell AD (2013) CHARMM36 All-atom additive protein force field:
583 Validation based on comparison to NMR data. J Comput Chem 34:2135-2145. doi:
584 10.1002/jcc.23354

585 Katoh K, Standley DM (2013) MAFFT multiple sequence alignment software version 7:
586 Improvements in performance and usability. Mol Biol Evol 30:772-780. doi:
587 10.1093/molbev/mst010

588 Kumar VP, Thomas LM, Bobyk KD, Andi B, Cook PF, West AH (2012) Evidence in support
589 of lysine 77 and histidine 96 as acid–base catalytic residues in saccharopine
590 dehydrogenase from *Saccharomyces cerevisiae*. Biochemistry 51:857-866. doi:
591 10.1021/bi201808u

592 Letunic I, Bork P (2024) Interactive Tree of Life (iTOL) v6: Recent updates to the
593 phylogenetic tree display and annotation tool. Nucleic Acids Res 52:W78-W82. doi:
594 10.1093/nar/gkae268

595 Li Y, Steenwyk JL, Chang Y, Wang Y, James TY, Stajich JE, Spatafora JW, Groenewald
596 M, Dunn CW, Hittinger CT, Shen X-X, Rokas A (2021) A genome-scale phylogeny of the
597 kingdom Fungi. Curr Biol 31:1653-1665.e5. https://doi.org/10.1016/j.cub.2021.01.074

MacKerell AD, Bashford D, Bellott M, Dunbrack RL, Evanseck JD, Field MJ, Fischer S, Gao J, Guo H, Ha S, Joseph-McCarthy D, Kuchnir L, Kuczera K, Lau FTK, Mattos C, Michnick S, Ngo T, Nguyen DT, Prodhom B, Reiher WE, Roux B, Schlenkrich M, Smith JC, Stote R, Straub J, Watanabe M, Wiórkiewicz-Kuczera J, Yin D, Karplus M (1998) All-atom empirical potential for molecular modeling and dynamics studies of proteins. J Phys Chem B 102:3586-3616. doi: 10.1021/jp973084f

Nachtweide S, Stanke M (2019) Multi-genome annotation with AUGUSTUS. In: Kollmar M (ed) Gene Prediction. Methods Mol Biol 1962:139-160. doi: 10.1007/978-1-4939-9173-0_8

Panasenko VT (1967) Ecology of microfungi. Bot Rev 33:189-215. doi: 10.1007/BF02858637

Salvadó Z, Arroyo-López FN, Guillamón JM, Salazar G, Querol A, Barrio E (2011) Temperature adaptation markedly determines evolution within the genus Saccharomyces. Appl Environ Microbiol 77:2292-2302. doi: 10.1128/AEM.01861-10

Saunders PP, Broquist HP (1966) Saccharopine, an intermediate of the aminoadipic acid pathway of lysine biosynthesis. J Biol Chem 241:3435-3440. doi: 10.1016/S0021-9258(18)96483-5

Tamang JP, Watanabe K, Holzapfel WH (2016) Review: Diversity of microorganisms in global fermented foods and beverages. Front Microbiol 7:377. doi: 10.3389/fmicb.2016.00377

van Kempen M, Kim SS, Tumescheit C, Mirdita M, Lee J, Gilchrist CLM, Söding J, Steinegger M (2024) Fast and accurate protein structure search with foldseek. Nat Biotechnol 42:243-246. doi: 10.1038/s41587-023-01773-0

Wong TKF, Ly-Trong N, Ren H, Demotte P, Baños H, Roger AJ, Susko E, Bielow C, De Maio N, Goldman N, Hahn MW, dos Reis M, Sy Vinh L, Huttley G, Lanfear R, Minh BQ (2026) IQ-TREE 3: Phylogenomic inference software using complex evolutionary models. Mol Biol Evol. 43:msag117. doi: 10.1093/molbev/msag117

Xu H, Alguindigue SS, West AH, Cook PF (2007) A proposed proton shuttle mechanism for saccharopine dehydrogenase from *Saccharomyces cerevisiae*. Biochemistry 46:871-882. doi: 10.1021/bi0619808

Xu H, Andi B, Qian J, West AH, Cook PF (2006a) The α-aminoadipate pathway for lysine biosynthesis in fungi. Cell Biochem Biophys 46:43-64. doi: 10.1385/CBB:46:1:43

630 Xu H, West AH, Cook PF (2006b) Overall kinetic mechanism of saccharopine
631 dehydrogenase from *Saccharomyces cerevisiae*. Biochemistry 45:12156-12166. doi:
632 10.1021/bi0610808

633 Zabriskie TM, Jackson MD (2000) Lysine biosynthesis and metabolism in fungi. Nat Prod
634 Rep 17:85-97. doi: 10.1039/A801345D

635

Supplementary Files

This is a list of supplementary files associated with this preprint. Click to download.

- SupplMaterials01082026A.pdf